Magnetic quantum oscillations and multiple holon pockets in underdoped $YBa_2Cu_3O_{6+y}$

Wei Chen[1], Oleg P. Sushkov[1], and Takami Tohyama[2]
[1] *School of Physics, University of New South Wales, Sydney 2052, Australia*
[2] *Yukawa Institute for Theoretical Physics, Kyoto University, Kyoto 606-8502, Japan*
(Dated: November 20, 2018)

We show that lightly doped $YBa_2Cu_3O_{6+y}$ has multiple holon pockets with different areas, which lead to multiple frequencies of magnetic quantum oscillations. Using neutron scattering data on incommensurate spin ordering we determine these areas, which yields frequencies in good agreement with experiments. Divergence of the effective mass observed in magnetic quantum oscillations indicates a quantum phase transition at the oxygen content $y \approx 0.48$. We argue that the transition is the onset of quasistatic incommensurate magnetic order predicted by theory and observed in neutron scattering.

PACS numbers: 74.25.Jb 71.18.+y 74.72.Gh 75.30.Fv

Topology of the Fermi surface is one of the central problems in the physics of cuprate superconductors. An undoped cuprate is antiferromagnetic Mott insulator. At a sufficiently small doping the system can be described by the extended two-dimensional t-J model [1, 2] that predicts small holon pockets located at the "nodal points". We use the term "holon" to stress that the quasiparticle does not carry usual spin, with more details to be explained later. On the other hand there is no doubt that at a sufficiently large doping the system behaves like a normal metal with a large Fermi surface and normal quasiparticles which carry simultaneously electric charge and spin S=1/2. Description of the transition between these two regimes is an open theoretical problem.

Angle resolved photoemission spectroscopy (ARPES) studies indicate a large Fermi surface in overdoped regime and formation of Fermi arcs in the underdoped regime [3]. On the other hand, recent magnetic quantum oscillation (MQO) data [4–12] taken in $YBa_2Cu_3O_{6+y}$(YBCO) indicate small Fermi pockets at $y < 0.66$ that corresponds to doping $x < 0.125$. Throughout the paper we denote doping by x and use results of Ref. 13 to relate the oxygen content y with the doping level x. Very recent ARPES studies [14, 15] also give some indications of small Fermi pockets. A theoretical interpretation of ARPES in terms of holons is a fairly involved issue. In a photoemission measurement partially separated spin and charge have to recombine to form a physical electron. So far the recombination amplitude has only been calculated for the parent Mott insulator [16]. In contrast, MQO is sensitive mainly to the electric charge, hence interpretation of MQO in terms of holons is straightforward. With tilted magnetic field MQO can also probe spin of the quasiparticle. A very recent measurement of this kind [10] indicates suppression of spin and hence supports the holon picture.

The sign of the Hall coefficient measured in Ref. 5 corresponds to electron pockets instead of hole ones. However, the field applied in the experiments is smaller than the critical field H_{c2}, hence the contribution from the vortex liquid has to be taken into account, which may alter sign of the Hall coefficient [17, 18]. In the present work we consider only hole pockets.

In this paper we address the following issues related to MQO: (1)Typically more than one MQO frequency is observed. What is the origin for the multiple frequencies? (2)The main MQO frequency corresponds to the area of the pocket about 1.8% of the Brillouin zone. How to reconcile this very small area with the Luttinger sum rule? (3)Divergence of the effective mass has been observed [11] at doping about 9%. What is the physical origin for this quantum critical point (QCP)?

We will relate MQO with recent neutron scattering observations [19–23]. These data demonstrate incommensurate spin ordering pined to the tetragonal a^* direction. Depending on doping the ordering can be static or dynamic. The QCP separating regions of dynamic and static ordering is located at $x_{\rm QCP} \approx 0.09$. The spin-wave pseudogap $\Delta_{\rm sw}$ is opened at $x > x_{\rm QCP}$. The data [19] on $YBa_2Cu_3O_{6.5}$ ($x \approx 0.1$) show $\Delta_{\rm sw} \sim 10$ meV, while in $YBa_2Cu_3O_{6.6}$ ($x \approx 0.12$) $\Delta_{\rm sw} \sim 20$ meV [20]. On the other hand the quasistatic scattering has been observed at $x < x_{\rm QCP}$ where $\Delta_{\rm sw} = 0$. In $YBa_2Cu_3O_{6.45}$ ($x \approx 0.085$) the signal is very weak [21, 22], and it is much bigger [23] in $YBa_2Cu_3O_{6.35}$ ($x \approx 0.065$).

MQO in a magnetic field B is described as $\cos(2\pi\frac{F}{B} + \phi)$. The period F and the area enclosed by a trajectory in the momentum space A_k are related as [24]

$$F = \frac{c\hbar}{2\pi e} A_k \ . \tag{1}$$

The typical measured value of F in YBCO is about 500 T, which gives a ratio of A_k to the total area of the Brillouin zone $A_{\rm BZ} = (2\pi/a)^2$ ($a = 3.81$ Å is the lattice spacing) to be $A_k/A_{\rm BZ} \approx 0.0176$.

Our analysis of MQO is based on the spin spiral theory of a lightly doped Mott insulator. While the idea of the spin spiral has been suggested quite some time

ago [25–28], the consistent theory with account of quantum fluctuations has been developed only recently [29]. Generalization of the spiral theory to bilayer YBCO has been discussed in Ref. 30. The theory is based on expansion in powers of doping x, so it is parametrically justified at $x \ll 1$. The theory is formulated in terms of the bosonic $\vec{n}$-field ($n^2 = 1$) that describes the staggered component of the copper spins, and in terms of fermionic holons ψ. The holon field ψ carries electric charge and it has a pseudospin that originates from two sublattices. Minima of the holon dispersion are at the nodal points $\mathbf{q}_0 = (\pm\pi/2, \pm\pi/2)$, so there are holons of two types ψ_α, $\alpha = 1, 2$, corresponding to two nodal directions. The dispersion in a pocket is somewhat anisotropic, but for simplicity we use here the isotropic approximation, $\epsilon(\mathbf{p}) \approx \beta \mathbf{p}^2/2$, where $\mathbf{p} = \mathbf{q} - \mathbf{q}_0$. Lattice spacing of the square lattice is set to be equal to unity $a = 3.81\,\text{Å} \to 1$. The effective Lagrangian for a single layer system reads [29]

$$\begin{aligned}
\mathcal{L} &= \frac{\chi_\perp}{2}\dot{\vec{n}}^2 - \frac{\rho_s}{2}(\nabla\vec{n})^2 + \sum_\alpha \{\frac{i}{2}[\psi_\alpha^\dagger \mathcal{D}_t \psi_\alpha - (\mathcal{D}_t\psi_\alpha)^\dagger \psi_\alpha] \\
&- \psi_\alpha^\dagger \epsilon(\mathcal{P})\psi_\alpha + \sqrt{2} g(\psi_\alpha^\dagger \vec{\sigma}\psi_\alpha)\cdot[\vec{n}\times(\mathbf{e}_\alpha\cdot\nabla)\vec{n}]\}\,, \\
\mathcal{P} &= -i\nabla + \frac{1}{2}\vec{\sigma}\cdot[\vec{n}\times\nabla\vec{n}]\,, \\
\mathcal{D}_t &= \partial_t + \frac{i}{2}\vec{\sigma}\cdot[\vec{n}\times\dot{\vec{n}}]\,. \qquad (2)
\end{aligned}$$

First two terms in the Lagrangian represent the usual nonlinear σ model, with magnetic susceptibility $\chi_\perp \approx 0.066J$ and spin stiffness $\rho_s \approx 0.175J$, where $J \approx 130$ meV is the antiferromagnetic exchange in the parent Mott insulator. The extended t-J model predicts the following values of the coupling constant and the inverse effective mass, $g \approx 1.0J$, $\beta \approx 2.5J$ ($m^* = 1.6m_e$). Below we will not use this value of β, instead we will treat β as a fitting parameter. The pseudospin operator is $\frac{1}{2}\vec{\sigma}$, and $\mathbf{e}_\alpha = (1/\sqrt{2}, \pm 1/\sqrt{2})$ is a unit vector orthogonal to the face of the magnetic Brillouin zone (MBZ) where the holon is located. Note that usage of the MBZ notations does not imply that there is a long range magnetic order. This is just a convenient way to avoid double counting of degrees of freedom, and the pseudospin accounts for doubling of the area of MBZ. Due to the MBZ notations one should consider two full pockets located at $\mathbf{q}_0 = (+\pi/2, -\pi/2)$ and $\mathbf{q}_0 = (+\pi/2, +\pi/2)$, hence the index α takes two values. We stress that it does not matter if the ground state expectation value of the n-field is nonzero, $\langle\vec{n}\rangle \neq 0$ (magnetic ordering), or zero, $\langle\vec{n}\rangle = 0$. The only condition for validity of Eq.(2) is that dynamic fluctuations of the $\vec{n}$-field are sufficiently slow. Typical energy scale of the $\vec{n}$-field quantum fluctuations is $E_{\text{cross}} \propto x^{3/2}$ (position of the neck of the "hour glass" spin wave dispersion), as discussed in Ref. 29, and it must be small compared to the holon Fermi energy $\epsilon_F \propto x$. The inequality $E_{\text{cross}} \ll \epsilon_F$ is valid up to optimal doping, $x \approx 0.15$, below which Eq.(2) is parametrically justified.

To account for the interaction with magnetic field, we make the following modifications in Eq.(2) [29]: A magnetic vector potential $\mathbf{A}$ is included in the long derivative $\mathcal{P} \to \mathcal{P} - \frac{e}{c}\mathbf{A}$, kinetic energy of $n-$field is modified $\dot{\vec{n}}^2 \to \left(\dot{\vec{n}} - [\vec{n}\times\vec{B}]\right)^2$, and an extra term $\delta\mathcal{L}_B = \frac{1}{2}(\vec{B}\cdot\vec{n})\psi_\alpha^\dagger(\vec{\sigma}\cdot\vec{n})\psi_\alpha$ is included. Here we include the Bohr magneton in definition of the magnetic field, $2\mu_B B \to B$. The precise meaning of spin-charge separation is clear under this context: In a normal Fermi liquid the spin interaction is $\delta\mathcal{L}_B^{\text{NFL}} = \frac{1}{2}\psi_\alpha^\dagger \vec{B}\cdot\vec{\sigma}\psi_\alpha$. In contrast, for a spin-spiral state the g-term in Eq.(2) enforces $\vec{n} \perp \vec{\sigma}$, hence the expectation value of $\delta\mathcal{L}_B$ goes to zero, $\langle(\vec{B}\cdot\vec{n})(\vec{\sigma}\cdot\vec{n})\rangle = 0$. Thus the pseudospin does not interact with magnetic field in the first order in B and this is the meaning of the spinless nature of the holon.

In the effective action (2) the ρ_s-term, the $\epsilon(\mathcal{P})$-term and the g-term are important in semiclassical approximation. All other terms contain time derivatives, which are important only for quantum fluctuations and we disregard them for now. For the single layer case, we choose the plane of the coplanar spin spiral to be the xy-plane in the spin space, $\vec{n} = (\cos\boldsymbol{Q}\cdot\boldsymbol{r}, \sin\boldsymbol{Q}\cdot\boldsymbol{r}, 0)$. Due to the g-term in Eq.(2) the psedospin of a holon is quantized along z-axis. Energy of the holon is $\epsilon(\mathbf{p}) = \pm gQ + \beta\mathbf{p}^2/2$, where $\pm gQ$ is the pseudospin splitting. The splitting between two pseudospin branches is shown in the left panel of Fig.1. Minimization of the semiclassical energy shows

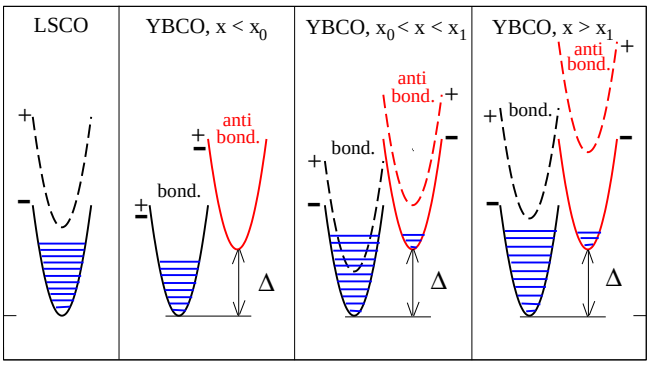

FIG. 1: (color online) Filling of holon bands. Left panel: single layer $La_{2-x}Sr_xCuO_4$ (LSCO). Three right panels: double layer YBCO in three different regimes. The solid and the dashed line correspond to different pseudospin projections, the splitting is $\pm gQ$. In the YBCO panels left/right parts show bonding/antibonding bands, the splitting is $\pm\Delta/2$.

that $\boldsymbol{Q}$ is directed along the CuO bond [$\boldsymbol{Q} \propto (1, 0)$ or $\boldsymbol{Q} \propto (0, 1)$] and has value $Q = \frac{g}{\rho_s}x$. The upper pseudospin branch of the holon dispersion is always empty, as shown in the left panel, Fig.1, hence the area of the holon pocket is $\frac{A_k}{A_{\text{BZ}}} = \frac{1}{2}x$. Quantum fluctuations reduce the static value of spin, $|\langle\vec{n}\rangle| < 1$, moreover, at $x > x_{\text{QCP}} \approx 0.1$ the expectation value of $\vec{n}$ vanishes, $\langle\vec{n}\rangle = 0$, and the spiral becomes fully dynamic [29]. However, this does

not influence the value of the incommensurate vector $\boldsymbol{Q}$ because the fluctuations are slow. The point is that the semiclassical analysis is based on relatively short distance and time, with corresponding typical momenta and energies $Q < q_{\rm semi} < p_F \propto \sqrt{x}$, $\omega_{\rm semi} \sim \epsilon_F \propto x$. Quantum fluctuations come from smaller momentum/energy scales $q_{\rm quant} < Q$, $\omega_{\rm quant} \propto x^{3/2}$, as discussed in Ref. 29.

In the double layer case, one has to include the interlayer hopping in the effective action (2). As a result, holon wave function ψ attains bonding/antibonding index with respect to the interlayer hybridization [30]. The holon energy at *each of the two nodal points* reads $\epsilon(\mathbf{p}) = \beta \mathbf{p}^2/2 \pm gQ \pm \Delta/2$, where $\pm gQ$ is the pseudospin splitting and $\pm\Delta/2$ is the antibonding(a)/bonding(b) splitting. Effectively there are *four* different bands per nodal direction ($b-$, $b+$, $a-$, $a+$), altogether *eight* bands. The filling configuration of these bands is determined by minimizing the semiclassical energy, which yields three different doping regimes [30]

$$\begin{aligned} &1)\ \ x < x_0\ , && Q = 0 \\ &2)\ \ x_0 < x < x_1\ , && Q = \frac{g}{\rho_s}\frac{x - \Delta/(\pi\beta)}{3 - 2\lambda} \\ &3)\ \ x > x_1\ , && Q = gx/\rho_s\ , \end{aligned} \qquad (3)$$

where $\lambda = 2g^2/(\pi\beta\rho_s)$. The points x_0 and x_1 are Lifshitz points. Filling configuration of these three regimes are shown in Fig.1. Areas of the filled holon pockets are

$$\begin{aligned} 1)\quad & A_{b-}/A_{\rm BZ} = A_{b+}/A_{\rm BZ} = x/2 \\ 2)\quad & A_{b-}/A_{\rm BZ} = x/3 + gQ/(3\pi\beta) + \Delta/(6\pi\beta) \\ & A_{b+}/A_{\rm BZ} = x/3 - 2gQ/(3\pi\beta) + \Delta/6\pi\beta) \\ & A_{a-}/A_{\rm BZ} = x/3 + gQ/(3\pi\beta) - \Delta/(3\pi\beta) \\ 3)\quad & A_{b-}/A_{\rm BZ} = x/2 + \Delta/(4\pi\beta) \\ & A_{a-}/A_{\rm BZ} = x/2 - \Delta/(4\pi\beta)\ . \end{aligned} \qquad (4)$$

Note that the total occupied area is $2x$ because there are two layers. From (4) we conclude that there is one MQO frequency in the first regime, three frequencies in the second regime, and two frequencies in the third regime. Let us consider two scenarios for the doping dependence of the hybridization splitting: (A) a constant gap $\Delta = \Delta_0$, (B) $\Delta = \Delta_0(1 + \nu x)$, since the splitting Δ is due to tunneling via interlayer oxygen chains [31], a linear dependence on doping is possible.

Values of the incommensurate wave vector Q determined by neutron scattering [19–21] are presented in Fig.2. Comparing Fig.2 with Eqs.(3) one finds $x_0 \approx 0.06$, $x_1 \approx 0.13$. Using Eqs.(3), we can determine parameters of the model. We fix $g = J$ and $\rho_s = 0.175J$, as they are predicted by the extended t-J model. Within the scenario (A) the fit gives, $\lambda = 1.23$, $\beta = 2.95J$ ($m^* = 1.35m_e$), $\Delta_0 = 0.556J$. Within the scenario (B), the data from Fig.2 are not sufficient to determine the additional parameter ν. However, we can assume that value of λ in

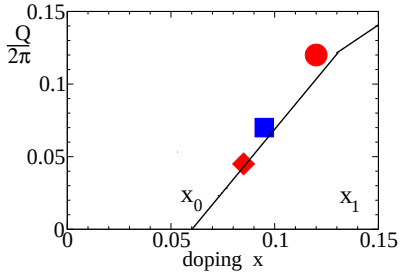

FIG. 2: (color online) Incommensurate wave vector versus doping. The blue square [19], the red circle [20], and the red diamond [21] show neutron scattering data. The solid line shows fit of the data using Eqs.(3).

YBCO and LSCO is the same, and use the value $\lambda = 1.31$ obtained in Ref. [29] from fitting the data for LSCO. This gives $\beta = 2.78J$ ($m^* = 1.43m_e$), $\Delta_0 = 0.37J$, $\nu = 6.9$ within the scenario (B). Note that values of β in both fits are close to that predicted by the extended t-J model, as demonstrated in the paragraph after Eq.(2), and the corresponding effective masses are close to that measured in MQO away from the QCP [11, 12], $m^* = 1.6 \pm 0.1m_e$.

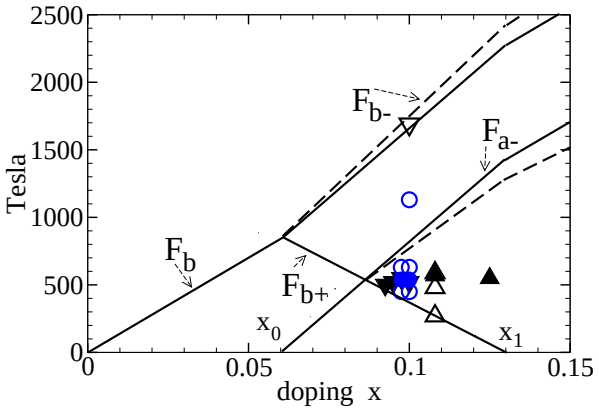

FIG. 3: (color online) Frequencies of MQO in Tesla versus doping. Solid lines show the theoretical prediction within the scenario (A), dashed lines show the prediction within the scenario (B). Predictions (A) and (B) coincide in the lower part of the figure. Experimental data are shown by symbols: Ref. [9] - blue circles, Ref. [11] - black triangles down, Ref. [12] - black triangles up. Full symbols correspond to maximum intensity lines.

Frequencies of MQO are determined by these parameters via Eqs.(4) and (1). The results are presented in Fig.3. Difference between the scenario (A) (solid lines) and the scenario (B) (dashed lines) is fairly small. There is quite a reasonable agreement with experimental data, especially having in mind that the theory has no fitting parameters related to MQO. Even a high frequency point $\approx 1690T$ is reproduced. Notice that MQO always contain higher harmonics. Most likely the blue circle at $\approx 1100T$ is such a harmonic [11]. Filling of each pocket is only a fraction of the total doping, this explains why the filling extracted from one single frequency seems to violate the Luttinger sum rule. The main frequency at $x \approx 0.09$ comes from the $b+$ pocket, which has Fermi

energy ≈ 40 meV, and the number of filled Landau levels at $B = 60$Tesla is $N = \epsilon_F/\hbar\omega_c \approx 6$, ω_c being the synchrotron frequency. Amplitude of MQO is proportional to $\exp\{-\pi\Gamma/\hbar\omega_c\}$, Ref. [32]. Assuming that the exponent is ~ 1, and relating the impurity broadening to the mean free path and to the Fermi velocity, $\Gamma = \hbar v_F/l$, we estimate the holon mean free path $l \sim 70a \sim 270$ Å.

A divergence of the effective mass at approaching $y = 0.49$ from higher doping has been reported [11]. The effective mass has been extracted via temperature dependence of the MQO signal. The divergence was interpreted [11] as a QCP due to a metal-insulator transition. Here we suggest an alternative explanation for this QCP, based on the current theory and on the evidences from neutron scattering. Besides the Lifshitz points x_0 and x_1, the spiral theory also predicts a QCP at $x_{\rm QCP} \approx 0.1$ which separates regions of static and dynamic spin spiral. The neutron scattering data [19–22] demonstrate this QCP in YBCO at doping level $x_{\rm QCP} \approx 0.09$, see discussion in the introduction. As one should expect, the precise position of this QCP depends on the applied magnetic field. The quasistatic neutron scattering in $YBa_2Cu_3O_{6.45}$ is enhanced in the field [22], which indicates that magnetic field shifts the QCP towards higher doping. Most likely in the field 60-80 Tesla used in MQO, the QCP is located between $YBa_2Cu_3O_{6.47}$ and $YBa_2Cu_3O_{6.49}$. The point is that the field is hardly sufficient to close the spin-wave pseudogap $\Delta_{\rm sw} \sim 10$ meV in $YBa_2Cu_3O_{6.5}$ [19]. The QCP is driven by the long-wave-length quantum fluctuations, while holon pockets are formed at a shorter semiclassical scale. Therefore MQO frequencies are not sensitive to the magnetic QCP.

Effective mass in a quantum field theory always depends on the momentum transfer q, $m^* \to m^*_q$. The effective mass extracted from fitting neutron scattering data is relevant to the semiclassical scale $q \sim p_F \propto \sqrt{x}$. This mass does not "see" the magnetic QCP. However, the amplitude of the MQO signal is formed at the length scale $l \sim 70a \sim 270$ Å, which corresponds to a very small q and the corresponding effective mass is sensitive to the magnetic QCP. It is known [33] that the quasiparticle residue Z vanishes at a magnetic QCP. Since $m^* \propto 1/Z$, this implies that the effective mass is diverging. Alternatively one can say that the holon scattering rate from critical magnons is diverging. This gives a natural explanation of the divergence observed in Ref. [11], and also explains why position of the QCP observed in neutron scattering coincides with that observed in MQO: they are the same QCP.

In summary, we explained the MQO frequencies based on the spin-spiral theory of lightly doped Mott insulator. Fit of the incommensurate neutron scattering data shown in Fig.2 determines free parameters of the theory, and allows us to calculate frequencies of MQO as functions of doping. In the doping region $0.06 < x < 0.13$ the theory predicts three different frequencies, which yields a fairly good agreement with current experimental data, Fig.3, and the Luttinger sum rule is reconciled. We also argue that the quantum critical point observed in magnetic quantum oscillations (divergence of the effective mass) is the same quantum critical point that is observed in neutron scattering, which signatures the onset of the static incommensurate magnetic order.

We thank D. Haug, V. Hinkov and B. Keimer for important discussions and for communicating unpublished data. We acknowledge useful comments by S. Borisenko and C. Zhang.

[1] P. W. Anderson, Science **235**, 1196 (1987).
[2] F. C. Zhang and T. M. Rice, Phys. Rev. B **37**, R3759 (1988).
[3] M. R. Norman *et al.*, Nature **392**, 157 (1998).
[4] N. Doiron-Leyraud *et al.*, Nature **447**, 565 (2007).
[5] D. LeBoeuf *et al.*, Nature **450**, 533 (2007).
[6] E. A. Yelland *et al.*, Phys. Rev. Lett. **100**, 047003 (2008).
[7] C. Jaudet *et al.*, Phys. Rev. Lett. **100**, 187005 (2008).
[8] S. E. Sebastian *et al.*, Nature **454**, 200 (2008).
[9] A. Audouard *et al.*, Phys. Rev. Lett. **103**, 157003 (2009).
[10] S. E. Sebastian *et al.*, arXiv:0907.2958 (2009).
[11] S. E. Sebastian *et al.*, arXiv:0910.2359 (2009).
[12] J. Singleton *et al.*, arXiv:0911.2745 (2009).
[13] R. Liang, D. A. Bonn, and W. N. Hardy Phys. Rev. B **73**, 180505(R) (2006).
[14] J. Meng *et al.*, Nature **462**, 335 (2009).
[15] R.-H. He *et al.*, arXiv:0911.2245.
[16] O.P. Sushkov, G.A. Sawatzky, R. Eder, and H. Eskes, Phys. Rev. B **56**, 11769 (1997).
[17] M. Galffy and E. Zirngiebl, Solid State Commun. **68**, 929 (1988); S. N. Artemenko, I. G. Gorlova and Y. I. Latyshev, JETP Lett. 49, 403 (1989).
[18] D. I. Khomskii and A. Freimuth Phys. Rev. Lett., **75**, 1384 (1995).
[19] C. Stock *et al.*, Phys. Rev. B **69**, 014502 (2004).
[20] V. Hinkov *et al.*, Nature Phys. **3**, 780 (2007).
[21] V. Hinkov *et al.*, C. T. Lin, and B. Keimer, Science 319, 597 (2008).
[22] D. Haug *et al.*, Phys. Rev. Lett. **103**, 017001 (2009).
[23] D. Haug, V. Hinkov, B. Keimer, private communication.
[24] J. M. Ziman, *Principles of the Theory of Solids*, Cambridge, University Press, 1972.
[25] B. I. Shraiman and E. D. Siggia, Phys. Rev. Lett. **61**, 467 (1988).
[26] J. I. Igarashi and P. Fulde, Phys. Rev. B **45**, 10419 (1992).
[27] A. V. Chubukov and K. A. Musaelian, Rev. B **51**, 12605 (1995).
[28] O. P. Sushkov and V. N. Kotov, Phys. Rev. B **70**, 024503 (2004).
[29] A. I. Milstein and O. P. Sushkov, Phys. Rev. B **78**, 014501 (2008).
[30] O. P. Sushkov, Phys. Rev. B **79**, 174519 (2009).
[31] O. K. Andersen, A. I. Liechtenstein, O. Jepsen, and F. Paulsen, J. Phys. Chem. Solids **56**, 1573 (1995).
[32] A. Wasserman, M. Springford, Adv. Phys. **45**, 471 (1996).

[33] M. Vojta, C. Buragohain, and S. Sachdev, Phys. Rev. B **61**, 15152 (2000); O. P. Sushkov, Phys. Rev. B **62**, 12135 (2000).